

MAPPING THE INNER ZODIACAL LIGHT WITH CLEMENTINE. J. M. Hahn, *Lunar and Planetary Institute, Houston TX 77058, USA, (hahn@lpi.usra.edu)*, H. A. Zook, *NASA Johnson Space Center, Houston TX 77058, USA, (herbert.a.zook1@jsc.nasa.gov)*, B. Cooper, *Oceaneering Space Systems, Houston TX 77058, USA, (bcooper@oss.oceaneering.com)*, B. Sunkara, *University of Houston, Houston TX 77058, USA, (sunkara@lpi.usra.edu)*.

The zodiacal light is the sunlight that is reflected by interplanetary dust. This diffuse band of light is of considerable scientific interest, not just because its large extent actually makes it the most luminous component of our planetary system, but also because its distribution upon the sky is indicative of the spatial distribution of dust throughout the solar system. In order to assess that dust distribution, numerous observations have measured the brightness of the zodiacal light on various parts of the sky. Most notable are the infrared observations by the IRAS and COBE spacecraft which have produced fairly complete maps of the outer zodiacal light (e.g. radiation from dust exterior to Earth's orbit about the Sun) [1, 2]. However maps of the inner zodiacal light are generally less comprehensive. This is partly due to the difficulty of observing towards the Sun from the ground, since sunlight scattered by the atmosphere tends to mask the faint zodiacal light and contaminate the result, even when observing from aircraft or during eclipse.

However the situation improves considerably when observing from space. For instance, MacQueen *et al.* (1973) extracted wide-angle maps of the zodiacal light from photographs acquired by Apollo 16 astronauts while in lunar orbit, and the Helios 1 and 2 spacecraft sampled the zodiacal light brightness over heliocentric distances of 0.3 to 1.0 AU [4]. But it should be noted that the Apollo observations were of fairly low angular resolution, and the photometers onboard the spinning Helios spacecraft could only sample the zodiacal light along discrete latitudes on the sky.

However a considerable advance in sensitivity, angular resolution, and sky-coverage was achieved when the Clementine spacecraft used its navigation cameras to map the inner zodiacal light while in lunar orbit in early 1994. Using the Moon to eclipse the Sun, the spacecraft's star-tracker cameras repeatedly imaged the inner zodiacal light while the Sun was just below the lunar limb. The star-tracker camera has a very wide field of view, 29 by 44 degrees, and it was able to image the zodiacal light between the orbit of Venus down to about 7 solar radii (image saturation prevents us from viewing closer than about 2° from the Sun). Hundreds of such images were acquired in a broad visual band spanning wavelengths of 0.4 to 1.1 microns during Clementine's 71 days in orbit about the Moon, and a sample image can be found in [5].

These Clementine data require special processing since the images were acquired by a shutterless CCD camera. Because the camera's pixels are continuously exposed, the act of reading out the array along the CCD columns has the effect of briefly exposing each pixel to all parts of the sky subtending the same CCD column. Consequently, bright objects like the planet Venus, the illuminated Moon, and the core of the zodiacal light, all appear in the raw data as if smeared along the CCD columns. However the startracker readout time is known, so the magnitude of this 'streaking' can be inferred from the

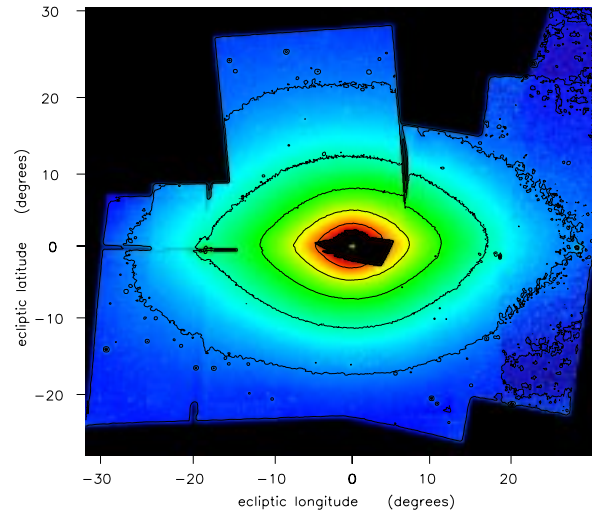


Figure 1: A mosaic of six fields-of-view of the inner zodiacal light acquired by the Clementine star tracker camera. The black regions indicate zones eclipsed by the Moon, saturated pixels or otherwise faulty data that are discarded. Ecliptic north and east are up and left. Adjacent isophotes differ by a factor of 3 in brightness. A saturated Venus at a longitude of $\lambda \simeq -20^\circ$ bled into surrounding pixels and perturbed the isophotes there. These six fields were acquired between March 5 and April 3 of 1994. Several other planets are also imaged (some at multiple epochs): Saturn at $\lambda \simeq -10^\circ$, Mars and Saturn at $\lambda \simeq 17^\circ$, and Mercury at $\lambda \simeq 27^\circ$. The westernmost fields have the shortest exposure times and the lowest signal/noise.

raw data itself, and the intrinsic image is recovered using the destreaking algorithm given in [5].

The Clementine images examined here are destreaked, have had their dark-current removed, and are flatfielded. Background stars and planets are also used to determine the camera's pointing, and the apparent brightness of solar-type field stars are used to calibrate these data. Although the Moon subtends a wide swath of the zodiacal light in each image, typically $\sim 20^\circ$, it blocks out different parts of the zodiacal light in images acquired at different times due to the relative motions of the spacecraft, the Moon, and the Sun. These images are then combined into a larger Sun-centered mosaic (Fig. 1), which shows the inner zodiacal light as would be seen by a virtual camera having a larger 60° field of view.

The mean surface brightness of the zodiacal light along the ecliptic, $Z(\epsilon)$, is plotted versus elongation angle ϵ in Fig. 2. The brightness of the zodiacal light in a given direction is the

REFERENCES

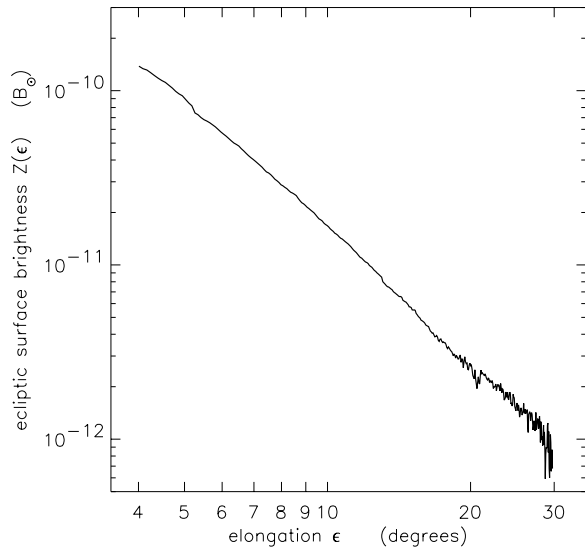


Figure 2: The surface brightness profiles $Z(\epsilon)$ of the zodiacal light east and west of the Sun along the ecliptic have been extracted from Fig. 1; this figure shows the averaged brightness Z in units of mean solar brightness B_{\odot} versus elongation angle ϵ .

dust surface area \times its reflected light scattering function, integrated along the line of sight. If it is assumed that the spatial density of the dust cross-section, $\sigma(r)$, has a power-law dependence upon heliocentric distance r as $\sigma(r) = \sigma_1(r/r_1)^{-\nu}$, then the zodiacal light's integrated surface brightness is [6]

$$Z(\epsilon) = \frac{\sigma_1 r_1 B_{\odot}}{\sin^{\nu+1} \epsilon} \Omega_{\odot} \int_{\epsilon}^{\pi} \Phi(\theta) \sin^{\nu} \theta d\theta, \quad (1)$$

where $\Omega_{\odot} = 6.80 \times 10^{-5}$ sr is the solid angle subtended by the Sun at the reference distance $r_1 = 1$ AU, $B_{\odot} = L_{\odot}/4\pi r_1^2 \Omega_{\odot} = 2.01 \times 10^{10}$ ergs/sec/cm²/sr is the mean solar brightness where L_{\odot} is the solar luminosity, $\Phi(\theta)$ is the scattering function for interplanetary dust, and θ is the scattering angle (e.g., $\theta = \pi - \alpha$ where α is the Sun—dust—observer phase angle). A power-law fit to Fig. 2 gives $Z(\epsilon) \simeq 2.36 \times 10^{-13} B_{\odot} / \sin^{2.4} \epsilon$ over elongations of $\epsilon < 13^{\circ}$, so $\nu \simeq 1.4$. Note that Fig. 2 does not show any evidence for a forward-diffraction component in the zodiacal light that would fall off as ϵ^{-3} when observed at sufficiently small elongation angles.

We employ the empirical scattering function

$$\Phi(\theta) = \frac{p}{\pi} e^{-K(\pi-\theta)} \text{sr}^{-1} \quad (2)$$

where p is the dust geometric albedo and the constant $K = 0.77$. This simple form for $\Phi(\theta)$ accurately reproduces the

zodiacal light brightness $Z(\epsilon)$ observed by other astronomers over a wide range of angles ϵ [7]. For $\Phi(\theta)$ having the form given in Eq. (2), the integral in Eq. (1) is quite insensitive to ϵ for the elongation angles $\epsilon < 30^{\circ}$ considered here, and it evaluates to $0.568p/\pi \text{sr}^{-1}$.

Inserting this result into Eq. (1) and equating that to the power-law fit to Fig. 2 yields $p\sigma_1 r_1 \simeq 1.9 \times 10^{-8}$. If we adopt a typical asteroid albedo of $p \simeq 0.08$, then the estimated density of the local dust cross-sectional area at $r_1 = 1$ AU is $\sigma_1 \simeq 1.6 \times 10^{-20} \text{cm}^2/\text{cm}^3$. Actually, the particular dust albedo used here was deliberately chosen so that σ_1 also agrees with measurements of dust impacts upon spacecraft [8]. Most of the interplanetary dust cross-section is contributed by grains having radii $R \sim 30 \mu\text{m}$ [8], so the number-density of these grains is $n \sim \sigma_1/\pi R^2 \sim 6 \times 10^{-16}$ which have a mass-density of $\sim 4\pi\rho R^3 n/3 \sim 1 \times 10^{-22} \text{gm}/\text{cm}^3$ for an assumed dust bulk-density of $\rho \sim 2 \text{gm}/\text{cm}^3$. This mass-density estimate is of course a lower limit since these observations are insensitive to the rarer grains much larger than $R \sim 30 \mu\text{m}$ that might contribute very little cross-sectional area yet may still carry a significant amount of unseen mass.

These findings should be regarded as preliminary estimates since we are still improving the the data-reduction and its calibration. Once that has been completed, we will build a three-dimensional model of the dust spatial density, which when applied to the two-dimensional zodiacal light map of Fig. 1, will be used to simultaneously extract both the horizontal and the vertical distributions of dust throughout the inner solar system.

References

- [1] Sykes, M. V., 1988, *Ap. J.*, **334**, L55.
- [2] Kelsall, T. *et al.*, 1988, *Ap. J.*, **508**, 44.
- [3] MacQueen, R. M., L. L. Ross, and T. Mattingly, 1973, *Planet. Space Sci.*, **21**, 2173.
- [4] Leinert, C., I. Richter, E. Pitz, and B. Planck, 1981, *Astron. Astrophys.*, **103**, 177.
- [5] Zook, H. A., B. L. Cooper, and A. E. Potter, 1997, *Lunar and Planetary Science Conference XXVIII*, 1103.
- [6] Hong, S. S., 1985, *A&A*, **146**, 67.
- [7] Zook, H. A. and D. J. Kessler, *OART-OSSA Meteoroid Environment Workshop*, 355.
- [8] Zook, H. A., R. E. Flaherty, and D. J. Kessler, 1970, *Plan. Space Sci.*, **18**, 953.